

---

# PULLING BACK THE CURTAIN ON RELU NETWORKS

---

**Maciej Satkiewicz**

314 Foundation, Kraków

maciej.satkiewicz@314.foundation

## ABSTRACT

Since any ReLU network is piecewise affine, its hidden units can be characterized by their pullbacks through the active subnetwork, i.e., by their gradients (up to bias terms). However, gradients of deeper neurons are notoriously misaligned, which obscures the network’s internal representations. We posit that models do align gradients with data, yet this is concealed by the intrinsic noise of the ReLU hard gating. We validate this intuition by applying soft gating in the backward pass only, reducing the local impact of weakly excited neurons. The resulting modified gradients, which we call *excitation pullbacks*, exhibit striking perceptual alignment on a number of ImageNet-pretrained architectures, while the rudimentary pixel-space gradient ascent quickly produces easily interpretable input- and target-specific features. Inspired by these findings, we formulate the *path stability* hypothesis, claiming that the binary activation patterns largely stabilize during training and get encoded in the pre-activation distribution of the final model. When true, excitation pullbacks become aligned with the gradients of a kernel machine that mainly determines the network’s decision. This provides a theoretical justification for the apparent faithfulness of the feature attributions based on these pullbacks, potentially even leading to mechanistic interpretability of deeper models. Incidentally, we give a possible explanation for the effectiveness of Batch Normalization and Deep Features, together with a novel perspective on the network’s internal memory and generalization properties. We release the code and an interactive app for easier exploration of the excitation pullbacks.

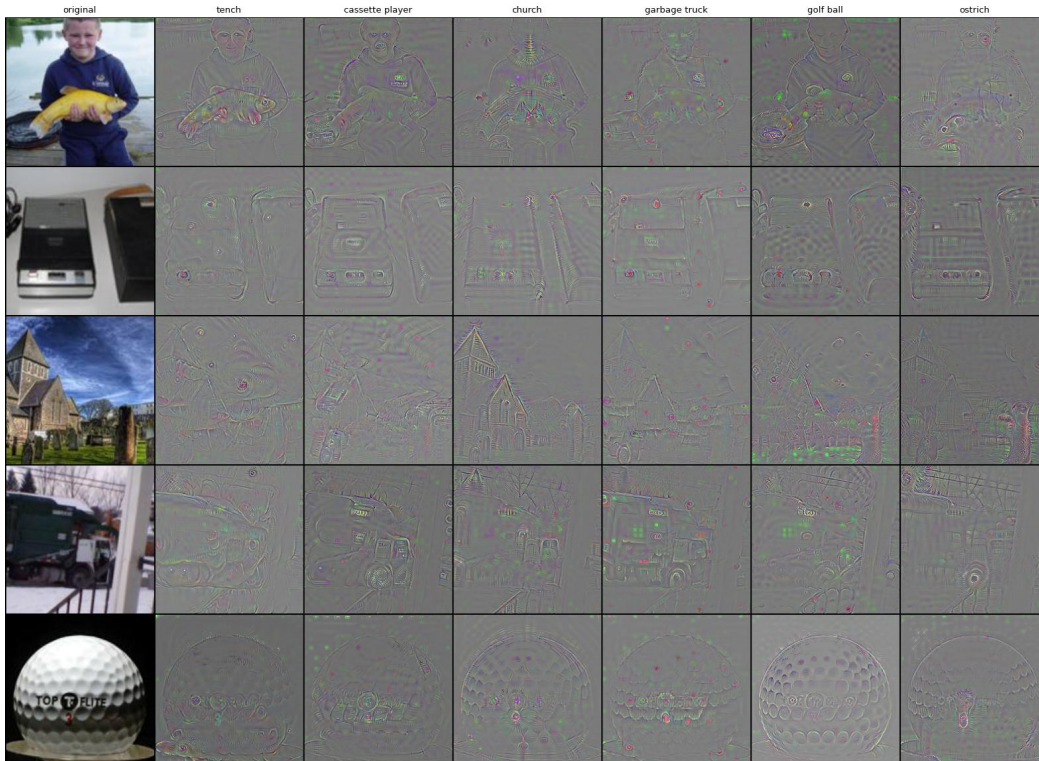


Figure 1: A rudimentary 5-step pixel-space gradient ascent guided by excitation pullbacks for pre-trained ResNet50. Each cell shows the difference between the perturbed and clean image, targeting the class in the column. Diagonal: original class; off-diagonal: counterfactuals. Last column: randomly selected extra label. See Section 6 for details. Best viewed digitally.

## 1 Introduction

Understanding how neural networks organize their internal representations remains a longstanding and fundamental challenge in deep learning. In this paper we report the results of a less common line of research, where our primary goal was not incremental leaderboard improvement, but rather breaking through conceptual barriers. We’ve published<sup>1</sup> the weekly research log to facilitate the discussion on this style of scientific inquiry. While we reduce the problem space to ReLU convolutional networks for vision tasks, our methods likely generalize to other activations with similar gating behavior, and potentially offer insights into a broader range of architectures and modalities.

We originally set out by experimenting with prototypical-part based models such as ProtoPNet [Chen et al., 2019]. However, this method of constructing self-explainable networks seems to have an unredeemable limitation in that it hinges on the black-box encoder network. To address this, we shifted our focus toward simpler, mechanistically interpretable architectures on CIFAR-10, with the goal of achieving gradient-data alignment. These experiments revealed an intriguing phenomenon: avoiding spatial gradient interference leads to substantially more interpretable gradients. Through a series of ablation studies, we then discovered that it is in fact possible to recover interpretable gradients in standard convolutional architectures by simply modifying the backward pass, leaving the forward computation intact. This led us to introduce what we call *excitation pullbacks*. The method turned out to scale to widely used ImageNet-pretrained architectures - including non-ReLU ones. However, we intentionally restrict the scope of this work to the following architectures: ResNet50 [He et al., 2015], VGG11\_BN [Simonyan and Zisserman, 2015], and DenseNet121 [Huang et al., 2018]; for reasons detailed in Section 6.

The striking perceptual alignment of excitation pullbacks strongly suggests a deeper cause. Our primary concern was to validate theoretically that the produced explanations are reasonably faithful to the network’s decision process. Building on our previous investigations we developed a formal framework that allows us to analyze the pullbacks from the path perspective, where *path* is any sequence of neurons selected from the consecutive layers. In particular, we observe that ReLU networks correspond to linear models in the path space (the Hilbert space of formal linear combinations of all paths), under a feature map given by the tensor product of the binary activation vectors (encoding the on/off states of neurons) of subsequent layers (see Section 3 for details). This made us suspect that these feature maps might largely stabilize during training in the form of a higher-rank tensor field, which we call a *path tensor feature* (see Hypothesis 1). If that’s indeed the case, then the network behaves like a piecewise linear kernel machine with excitation pullbacks approximating directionally it’s gradient, so that the feature attributions they produce can be considered faithful to the network’s internal circuitry. This would translate to excitation pullbacks constituting a mechanistic interpretation of deep models in a style reminiscent of the “neural circuits” program [Cammarata et al., 2020] - but considerably streamlined by the pullback computation.

Incidentally, the above considerations provide a possible explanation for the widespread effectiveness of Batch Normalization [Ioffe and Szegedy, 2015] in accelerating training, as normalizing neural activations significantly speeds up the stabilization of activation patterns and, consequently, the emergence of the path tensor feature and the global linear structure of the network’s internal representations, see Section 5.3. Furthermore, the success of Deep Features [Zhang et al., 2018] as a perceptual metric could be attributed to its kernel structure and the close relation to the path tensor feature (see Section 5.2). Interestingly, path tensor features allow us to view neural networks as associative memory systems, with excitation pullbacks as their contents (Section 5.4).

Our work demonstrates that standard pretrained networks do in fact align gradients with data, and highlights how one can extract interpretable representations of hidden neurons. Furthermore, the proposed formal framework sheds light on the internal organization of neural networks, and even offers a potential explanation for their generalization capabilities: if the stability condition expressed in Hypothesis 1 is satisfied, then the network’s decisions can be well approximated by a kernel machine whose gradient is feasibly accessible by the excitation pullback. The striking perceptual alignment observed in our experiments strongly suggests that this may indeed be the case, at least to some extent.

The paper is organized as follows:

Section 2 introduces necessary notions and notational conventions; in particular, the gating function and gating-induced pullbacks; Section 3 defines tensor field pullbacks and shows that ReLU networks correspond to linear maps in the path space; Section 4 introduces the excitation pullbacks and discusses the inherent gradient noise; Section 5 discusses the path stability hypothesis and its implications; Section 6 details the pullback visualization method used in the paper; Section 7 describes the related works and discusses the limitations of presented approach.

We release the code<sup>2</sup> and the interactive demo app<sup>3</sup> to make the exploration of excitation pullbacks easily accessible.

## 2 Preliminaries and notational conventions

This section establishes important notions and conventions used throughout the rest of the paper.

<sup>1</sup>[github.com/314-Foundation/ResearchLog](https://github.com/314-Foundation/ResearchLog)

<sup>2</sup>[github.com/314-Foundation/ExcitationPullbacks](https://github.com/314-Foundation/ExcitationPullbacks)

<sup>3</sup>[huggingface.co/spaces/msat/ExcitationPullbacks](https://huggingface.co/spaces/msat/ExcitationPullbacks)

## 2.1 ReLU networks

Let  $M$  be a feedforward ReLU network with parameters  $\theta \in \mathbb{R}^{d_{net}}$ , expressible as a composition of affine transformations and pointwise ReLU nonlinearities.<sup>4</sup> Let  $L$  denote the number of layers, and let  $d_\ell$  be the width of the  $\ell$ -th layer, with  $d_0$  denoting the input dimension. Let  $x_0$  denote the identity function on  $\mathbb{R}^{d_0}$ , i.e.  $x_0(x) := x$ . The network applies the following operations:

$$z_\ell := W_\ell x_{\ell-1} + b_\ell, \quad x_\ell := \text{ReLU}(z_\ell), \quad \text{for } \ell = 1, \dots, L$$

where  $W_\ell \in \mathbb{R}^{d_\ell \times d_{\ell-1}}$ ,  $b_\ell \in \mathbb{R}^{d_\ell}$ , and  $\text{ReLU}(z) = \max(0, z)$  is applied element-wise. We identify  $M$  with the overall network function  $x_L : \mathbb{R}^{d_0} \rightarrow \mathbb{R}^{d_L}$ , i.e.,  $M(x) := x_L(x)$ . We'll often abuse the notation and write  $x_\ell \in \mathbb{R}^{d_\ell}$ , meaning the value of  $x_\ell(x)$  for some fixed  $x \in \mathbb{R}^{d_0}$ ; same for  $z_\ell$  and other similar functions.

In this paper we'll treat  $M$  as backbone for some linear model, i.e.  $x_L$  represents a penultimate layer in some chosen architecture. Specifically, we'll consider  $f : \mathbb{R}^{d_0} \rightarrow \mathbb{R}$  defined by:

$$f_c := y_c^\top M$$

where  $y_c$  is a trainable set of weights  $y_c \in \mathbb{R}^{d_L}$  (a neuron in the network's head) and  $y_c^\top$  is its corresponding covector, i.e. the linear action of  $y_c$  on  $\mathbb{R}^{d_L}$  by the dot product:  $y_c^\top x = \langle y_c, x \rangle$ . Standard classification network with  $C$  classes has  $C$  corresponding vectors  $y_c$ . We will usually skip the lower index  $c$  assuming that it's fixed.

For notational brevity, we consider augmented matrices and vectors where the bias term is incorporated by appending a 1 to the end of the input vector. Specifically, we define the augmented input and weight matrix as

$$\tilde{x}_{\ell-1} := \begin{bmatrix} x_{\ell-1} \\ 1 \end{bmatrix} \in \mathbb{R}^{d_{\ell-1}+1}, \quad \tilde{W}_\ell := \begin{bmatrix} W_\ell & b_\ell \\ 0 & 1 \end{bmatrix} \in \mathbb{R}^{(d_\ell+1) \times (d_{\ell-1}+1)}$$

Then, the augmented pre-activation vector is given by

$$\tilde{z}_\ell := \tilde{W}_\ell \tilde{x}_{\ell-1}$$

### Conventions

Throughout the paper, we will often abuse notation by omitting the tilde and the explicit increase of dimension, writing simply

$$z_\ell = W_\ell x_{\ell-1}$$

with the understanding that the bias is included in the matrix  $W_\ell$  and the input vector  $x_{\ell-1}$ . We will occasionally write  $\mathbb{R}^{d_0^*} \subset \mathbb{R}^{d_0}$  to denote the true input space (without the implicitly added coordinate). Notice that  $\mathbb{R}^{d_0^*}$  remains the actual domain of  $f$ , as the extra coordinate is fixed.

## 2.2 Gating representation of ReLU networks

In ReLU networks, each activation can be equivalently viewed as a gating mechanism applied to the pre-activations. Specifically, for every layer  $\ell \in \{1, \dots, L\}$ , the activation function

$$x_\ell = \text{ReLU}(z_\ell)$$

can be rewritten as

$$x_\ell = g_\ell \odot z_\ell$$

where  $\odot$  is the Hadamard product and  $g_\ell \in \{0, 1\}^{d_\ell}$  is a binary gating vector defined by

$$g_\ell[i] = \begin{cases} 1 & \text{if } z_\ell[i] > 0, \\ 0 & \text{otherwise.} \end{cases}$$

Since  $g_\ell$  is itself a function of the input  $x$ , we may define the *gating* function:

$$G : \mathbb{R}^{d_0} \rightarrow \prod_{\ell=1}^L \{0, 1\}^{d_\ell}, \quad G(x) := (g_1(x), \dots, g_L(x)) \quad (1)$$

Let  $G_\ell(x) = \text{diag}(g_\ell(x)) \in \{0, 1\}^{d_\ell \times d_\ell}$  denote the diagonal matrix whose diagonal entries are given by  $g_\ell(x)$ . Then, the network output can be written as a product of (augmented) weight matrices interleaved with input-dependent diagonal matrices:

$$M(x) = G_L(x)W_L G_{L-1}(x)W_{L-1} \cdots G_1(x)W_1 x$$

<sup>4</sup>we omit max-pooling layers from the analysis to improve clarity, noting that similar arguments are likely to apply due to the structural similarity between max-pooling and ReLU; see Section 6.3.

where each  $W_\ell$  includes the bias terms via the convention introduced earlier.

This representation makes the piecewise-linear structure of ReLU networks explicit: for a fixed input  $x$ , the gating pattern  $(g_1, \dots, g_L) \in \prod_{\ell=1}^L \{0, 1\}^{d_\ell}$  determines a purely linear computation.

Similarly, let's define the *pre-activation function* as:

$$Z : \mathbb{R}^{d_0} \rightarrow \prod_{\ell=1}^L \mathbb{R}^{d_\ell}, \quad Z(x) := (z_1(x), \dots, z_L(x)) \quad (2)$$

i.e. the concatenation of all pre-activations of  $M(x)$ .

### 2.3 Gating-induced networks

More generally, given any gating function:

$$\Lambda : \mathbb{R}^{d_0} \rightarrow \prod_{\ell=1}^L [0, 1]^{d_\ell}, \quad \Lambda := (\lambda_1, \dots, \lambda_L), \quad \lambda_\ell : \mathbb{R}^{d_0} \rightarrow [0, 1]^{d_\ell} \quad (3)$$

we can define the  $\Lambda$ -induced network as

$$M_\Lambda(x) := \Lambda_L(x)W_L\Lambda_{L-1}(x)W_{L-1} \cdots \Lambda_1(x)W_1x \quad (4)$$

where  $\Lambda_\ell(x) = \text{diag}(\lambda_\ell(x)) \in [0, 1]^{d_\ell \times d_\ell}$  is the diagonal matrix formed from  $\lambda_\ell(x)$ . In particular,  $M$  is  $G$ -induced, i.e.  $M = M_G$ . Note that  $M_\Lambda$  implicitly depends on the network parameters  $\theta$ .

We can also define the matrix field  $\vec{M}_\Lambda : \mathbb{R}^{d_0} \rightarrow \mathbb{R}^{d_L} \times \mathbb{R}^{d_0}$  by:

$$\vec{M}_\Lambda(x) := \Lambda_L(x)W_L\Lambda_{L-1}(x)W_{L-1} \cdots \Lambda_1(x)W_1 \quad (5)$$

so that  $M_\Lambda(x) = \vec{M}_\Lambda(x)x$ . We set  $f_\Lambda := y^\top M_\Lambda$  and therefore  $f = f_G$ .

### 2.4 Pullbacks and vector fields

Note: the symbols in this subsection 2.4 are unrelated to the rest of the section 2.

Let  $f : \mathbb{R}^n \rightarrow \mathbb{R}$  be a scalar-valued function, and let  $\phi : \mathbb{R}^{d_0} \rightarrow \mathbb{R}^n$  be a map. The *pullback* of  $f$  through  $\phi$ , denoted  $\phi^*f$ , is defined as the composition

$$\phi^*f := f \circ \phi$$

which is a function  $\phi^*f : \mathbb{R}^{d_0} \rightarrow \mathbb{R}$  given explicitly by

$$(\phi^*f)(x) = f(\phi(x))$$

This construction allows us to view  $f$  as a scalar function defined directly on the domain  $\mathbb{R}^{d_0}$  (through the action of  $\phi$ ).

#### Convention

Whenever a piecewise continuous vector field  $v : \mathbb{R}^{d_0} \rightarrow \mathbb{R}^{d_0}$  satisfies

$$\langle v(x), x \rangle = v^\top(x)x = f(\phi(x)) = (\phi^*f)(x)$$

we will refer both to  $v$  and its corresponding covector field  $v^\top : \mathbb{R}^{d_0} \rightarrow (\mathbb{R}^{d_0})^*$  as pullbacks (of  $f$  through  $\phi$ ).

### 2.5 Gating-induced pullbacks

We can pull the linear map  $y^\top : \mathbb{R}^{d_L} \rightarrow \mathbb{R}$  back to the input space  $\mathbb{R}^{d_0}$  through  $M_\Lambda$ , generating the following covector field over  $\mathbb{R}^{d_0}$ :

$$v_\Lambda^\top := y^\top \vec{M}_\Lambda \quad (6)$$

We will call both  $v_\Lambda^\top$  and the corresponding vector field  $v_\Lambda$  a  $\Lambda$ -pullback. In particular, we have  $v_G^\top = y^\top \vec{M}_G$ . The following sequence of equations can be easily verified:

$$f_\Lambda(x) = y^\top M_\Lambda(x) = y^\top \vec{M}_\Lambda(x)x = v_\Lambda^\top(x)x = \langle v_\Lambda(x), x \rangle \quad (7)$$

This means that  $f_\Lambda$  is represented by its  $\Lambda$ -pullback  $v_\Lambda$ .

Now, since  $f$  is locally affine in  $\mathbb{R}^{d_0^*}$  (see Section 2.1), then:

$$\nabla f = \nabla f_G = (y^\top \vec{M}_G)|_{\mathbb{R}^{d_0^*}} = (v_G^\top)|_{\mathbb{R}^{d_0^*}} \quad (8)$$

This means that  $v_G|_{\mathbb{R}^{d_0^*}}$  can be easily computed as the network's gradient.

### Note 2.1

The pullback representation is important for explainability as it expresses the network action as a dot product with a well-understood entity, i.e. an input-space vector (field).

## 2.6 Training dynamics

Network parameters  $\theta$  and  $u$  change during training. We index time steps by  $t \in \{0, \dots, T\}$ , where  $t = 0$  denotes the initialization and  $t = T$  corresponds to the final state of training. Whenever an upper index ( $t$ ) appears, it indicates the value of the corresponding object at training step  $t$ , for example  $(y^{(t)}, \theta^{(t)})$  denotes the network parameters and  $G^{(t)}$  denotes the gating function induced by  $M^{(t)}$ . For notational brevity, we omit the index  $t = T$  when referring to the final trained model.

## 3 The path space and tensor field pullbacks

### 3.1 Network action as atom filtering

Let's dive deeper into the structure of  $M$ . Fix a hidden neuron  $u_\ell[i]$ , i.e. the one corresponding to the  $i$ -th output in the  $\ell$ -th layer of  $M$ . Due to the compositional nature of the network, we can define the pullback  $v_\Lambda|_{(\ell, i)}$  of  $u_\ell[i]$  in the same way we did for  $y$  - just consider the appropriate subnetwork below  $u_\ell[i]$  as the backbone. Moreover, the full-network pullback  $v_\Lambda$  can be expressed as a weighted sum of the pullbacks of neurons from previous layers, for example:

$$v_\Lambda = \sum_{i=1}^{d_L} y[i] \cdot \lambda_L[i] \cdot v_\Lambda|_{(L, i)}$$

i.e.  $v_\Lambda$  is a weighted sum of layer- $L$  pullbacks. This means that neurons in layer  $L$  contribute particular directions  $v_\Lambda|_{(L, i)}$  to the full pullback  $v_\Lambda$ , weighted by  $\lambda_L[i]$ , giving an explicit sense to the intuition that neurons form a compositional hierarchy of feature detectors.

We can also express  $v_\Lambda$  as the weighted sum of first-layer pullbacks:

$$v_\Lambda = \sum_{(i_1, i_2, \dots, i_L)} y[i_L] \cdot \lambda_L[i_L] \cdot W_L[i_L, i_{L-1}] \cdots \lambda_2[i_2] \cdot W_2[i_2, i_1] \cdot \lambda_1[i_1] \cdot v_\Lambda|_{(1, i_1)}$$

Where  $(i_1, \dots, i_L)$  is the *path* through layers  $1, \dots, L$ , i.e. the selection of indices  $i_\ell \in \{1, \dots, d_\ell\}$ . Now let's rearrange the factors:

$$v_\Lambda = \sum_{(i_1, i_2, \dots, i_L)} \left( \prod_{\ell=1}^L \lambda_\ell[i_\ell] \right) \left( y[i_L] \prod_{\ell=2}^L W_\ell[i_\ell, i_{\ell-1}] \right) \cdot v_\Lambda|_{(1, i_1)}$$

Notice that  $v_G|_{(1, i_1)} = (W_1[i_1])^\top \in \mathbb{R}^{d_0}$ , i.e. it's a  $i_1$ -th row of  $W_1$ , so we have:

$$v_\Lambda = \sum_{(i_1, i_2, \dots, i_L)} \left( \prod_{\ell=1}^L \lambda_\ell[i_\ell] \right) \left( y[i_L] \prod_{\ell=2}^L W_\ell[i_\ell, i_{\ell-1}] \right) \cdot (W_1[i_1])^\top \quad (9)$$

Let  $\mathcal{P}_k = \{(p_k, \dots, p_L) : p_\ell \in \{k, \dots, d_\ell\}\}$  denote the set of all paths through layers  $k, \dots, L$ , fix  $p = (p_1, \dots, p_L) \in \mathcal{P}_1$  and define the *path activity* function  $\Lambda^p : \mathbb{R}^{d_0} \rightarrow [0, 1]$  as:

$$\Lambda^p(x) := \prod_{\ell=1}^L \lambda_\ell(x)[p_\ell] \quad (10)$$

We may now rewrite the Equation 9 as:

$$v_\Lambda(x) = \sum_{p \in \mathcal{P}_1} \Lambda^p(x) \cdot \left( y[p_L] \prod_{l=2}^L W_\ell[p_\ell, p_{\ell-1}] \right) (W_1[p_1])^\top \quad (11)$$

### Note 3.1

Equation 11 expresses  $v_\Lambda$  as a weighted sum of constant vector fields (*atoms*) indexed by  $\mathcal{P}_1$ , with the only dependence on  $x$  being via  $\Lambda^p$ . In case of  $\Lambda = G$  this amounts to filtering the atoms by an input-specific binary mask.

## 3.2 Tensor field pullbacks

Setting  $P_1 = |\mathcal{P}_1| = \prod_{\ell=1}^L d_\ell$  and choosing some enumeration of  $\mathcal{P}_1$  we may lift  $\Lambda^p$  to the function  $\tilde{\Lambda} : \mathbb{R}^{d_0} \rightarrow \mathbb{R}^{P_1}$  as:

$$\tilde{\Lambda}(x) := (\Lambda^p(x))_{p \in \mathcal{P}_1} \quad (12)$$

By construction,  $\tilde{\Lambda}(x)$  can be naturally identified with the tensor product of all  $\lambda_\ell(x)$ :

$$\tilde{\Lambda}(x) \cong \bigotimes_{\ell=1}^L \lambda_\ell(x) \in \bigotimes_{\ell=1}^L \mathbb{R}^{d_\ell} \cong \mathbb{R}^{P_1} \quad (13)$$

We will call  $\mathbb{R}^{P_1}$  a *tensor product* and refer to it's elements as *tensors*. Similarly,  $\tilde{\Lambda}$  will be called a *tensor field* over  $\mathbb{R}^{d_0}$ .

More generally, for any piecewise continuous tensor field  $\tau : \mathbb{R}^{d_0} \rightarrow [0, 1]^{P_1} \subset \mathbb{R}^{P_1}$  we can define  $\tau$ -pullback  $v_\tau : \mathbb{R}^{d_0} \rightarrow \mathbb{R}^{d_0}$  as the following vector field:

$$v_\tau(x) := \sum_{p \in \mathcal{P}_1} \tau_p(x) \cdot \left( y[p_L] \prod_{l=2}^L W_\ell[p_\ell, p_{\ell-1}] \right) (W_1[p_1])^\top \quad (14)$$

i.e.  $v_\tau(x)$  is the sum of atoms with weights determined by the tensor  $\tau(x) \in \mathbb{R}^{P_1}$ . Consequently, we may define the  $\tau$ -induced function  $f_\tau : \mathbb{R}^{d_0} \rightarrow \mathbb{R}$  as

$$f_\tau(x) := \langle v_\tau(x), x \rangle \quad (15)$$

It's easy to see that  $v_\Lambda = v_{\tilde{\Lambda}}$  and  $f_\Lambda = f_{\tilde{\Lambda}}$  (Equations 7, 11 and 12), so we may safely overload the notation.

### Note 3.2

$\tilde{\Lambda}(x) \in \bigotimes_{\ell=1}^L \mathbb{R}^{d_\ell}$  is a rank-1 tensor, while  $\tau(x)$  can have arbitrary rank.

## 3.3 Path space and the linear nature of ReLU networks

Consider  $\mathcal{P}_0$ , the set of all paths through layers  $0, \dots, L$  and  $p = (p_0, p_1, \dots, p_L) \in \mathcal{P}_0$ . Let  $p|_k := (p_k, \dots, p_L)$  denote the (unique) sub-path of  $p$  starting at layer  $k$ . We will abuse the notation and write  $\tau_p$  instead of  $\tau_{p|1}$ . With that remark we can expand  $f_\tau(x)$  as:

$$\begin{aligned} f_\tau(x) &= \langle v_\tau, x \rangle = \sum_{p \in \mathcal{P}_1} \tau_p(x) \cdot \left( y[p_L] \prod_{l=2}^L W_\ell[p_\ell, p_{\ell-1}] \right) \langle (W_1[p_1])^\top, x \rangle \\ &= \sum_{p \in \mathcal{P}_1} \tau_p(x) \cdot \left( y[p_L] \prod_{l=2}^L W_\ell[p_\ell, p_{\ell-1}] \right) \left( \sum_{i=1}^{d_0} W_1[p_1, i] \cdot x[i] \right) \\ &= \sum_{p \in \mathcal{P}_1} \sum_{i=1}^{d_0} \tau_p(x) \cdot x[i] \cdot \left( y[p_L] \prod_{l=2}^L W_\ell[p_\ell, p_{\ell-1}] \right) W_1[p_1, i] \\ &= \sum_{p \in \mathcal{P}_0} \tau_p(x) \cdot x[p_0] \cdot \left( y[p_L] \prod_{l=1}^L W_\ell[p_\ell, p_{\ell-1}] \right) \end{aligned}$$

Again, we call  $\mathbb{R}^{P_0}$  a *tensor product* as  $\mathbb{R}^{P_0} \cong \bigotimes_{\ell=0}^L \mathbb{R}^{d_\ell} \cong (\bigotimes_{\ell=1}^L \mathbb{R}^{d_\ell}) \otimes \mathbb{R}^{d_0}$ . Additionally, we refer to  $\mathbb{R}^{P_0}$  as the *path space*, as this is the space of all neural paths in the network.

Let's define  $\Omega : \mathbb{R}^{d_L} \times \mathbb{R}^{d_{net}} \rightarrow \mathbb{R}^{P_0}$  as:

$$\Omega((y, \theta)) := (\omega_p)_{p \in \mathcal{P}_0}, \quad \text{where } \omega_p := y[p_L] \prod_{\ell=1}^L W_\ell[p_\ell, p_{\ell-1}], \quad p = (p_0, p_1, \dots, p_L) \quad (16)$$

and a  $\tau$ -induced *feature function*  $\phi_\tau : \mathbb{R}^{d_0} \rightarrow \mathbb{R}^{P_0}$  as:

$$\phi_\tau(x) := (\tau_p \cdot x[p_0])_{p \in \mathcal{P}_0} \cong \tau \otimes x \quad (17)$$

We may now express  $f_\tau$  as a dot product in  $\mathbb{R}^{P_0}$ :

$$f_\tau(x) = \sum_{p \in \mathcal{P}_0} (\phi_\tau(x))_p \cdot \omega_p = \langle \phi_\tau(x), \omega \rangle \quad (18)$$

Observe that the dimension of  $\mathbb{R}^{P_0}$  scales multiplicatively with the network's depth and therefore, in deeper networks, it is orders of magnitude larger than the number of network parameters (which scales additively with depth). In a sense this means that neural networks, generally considered to be overparameterised models, are actually significantly underparameterised from the path space point of view.

Notice that the  $\tau$ -pullback defined earlier (Equation 14) is trivially equal to the pullback of  $\omega^\top : \mathbb{R}^{P_0} \rightarrow \mathbb{R}$  through the feature function  $\phi_\tau : \mathbb{R}^{d_0} \rightarrow \mathbb{R}^{P_0}$ , because, by Equations 15 and 18, we have:

$$\omega^\top(\phi_\tau(x)) = \langle \omega, \phi_\tau(x) \rangle = f_\tau(x) = \langle v_\tau(x), x \rangle \quad (19)$$

### Note 3.3

The equation 19 explicitly disentangles network's weights from the feature function, as, by definition,  $\omega$  does not depend on  $\tau$  and  $\phi_\tau$  does not depend on the network parameters  $(y, \theta)$ . This disentangled view suggests that most of the network's expressive power is due to the highly non-linear gating function  $G$ , as the network acts linearly (via  $\omega \in \mathbb{R}^{P_0}$ ) on inputs transformed by  $\phi_{\tilde{G}}$ . Moreover, by Equation 19, the action of  $\omega$  on  $\phi_{\tilde{G}}(x)$  can be directly visualised in the input space via the action of the pullback  $v_G$  on  $x$ . Even though  $\phi_{\tilde{G}^{(t)}}$  does change during training, it is significantly more stable than the direct mapping  $M_G^{(t)} : x \mapsto x_L^{(t)} \in \mathbb{R}^{d_L}$ , hinting at the importance of this representation.

## 4 Excitation pullbacks and the inherent gradient noise

### 4.1 On the inherent gradient noise

Despite the following representation property (see Equations 7 and 8):

$$f(x) = \langle v_G(x), x \rangle = v_G^\top(x)x$$

$$\nabla f(x) = v_G^\top(x)|_{\mathbb{R}^{d_0}^*}$$

the gradients of ReLU networks are notoriously hard to interpret (see Figure 2). This may suggest that those models rely on some strange predictive patterns that are meaningless to humans. But it may also mean that gradients are contaminated by an inherent noise that obfuscates a more regular underlying decision boundary. In this section, we advocate the latter view.

Indeed, by Equation 6 the pullback vector  $v_G(x)$ , and hence also the gradient  $\nabla f(x)$ , depend solely on the network parameters  $(y, \theta)$  and the gating pattern  $G(x)$ . This means that  $v_G(x)$  loses a lot of information about  $x$ , in particular about the pre-activation values  $z_\ell(x)$ . This loss of information might be important for the training process, as the network is less likely to overfit, but it is problematic for interpretability during inference.

To highlight the potential problems, suppose that  $x \in \mathbb{R}^{d_0}$  lies on the boundary of two linear regions of  $M$ . Let  $x_a \sim x$  and  $x_b \sim x$  be two nearby points lying on the opposite sides of the boundary, i.e. each in a different linear region. By continuity of  $f$ , we have

$$f(x_a) \approx f(x) \approx f(x_b)$$

which, by Equation 7, translates to

$$\langle v_G(x_a), x_a \rangle \approx \langle v_G(x), x \rangle \approx \langle v_G(x_b), x_b \rangle.$$

By properties of the dot product we get

$$\langle v_G(x_a), x \rangle \approx \langle v_G(x_b), x \rangle \implies \langle v_G(x_a) - v_G(x_b), x \rangle \approx 0 \quad (20)$$

This means that, in general, the pullback vectors  $v_G(x_a)$  and  $v_G(x_b)$  may differ significantly as long as their difference remains orthogonal to  $x$ , i.e. it can be any point from the entire hyperplane orthogonal to  $x$ . In standard training there is little incentive to align these orthogonal directions as they hardly affect the network’s value  $f(x)$  (incidentally, such incentive may be provided by adversarial training, see Section 7.1).

**Note 4.1**

Intuitively,  $v_G(x)$  may contain locally irrelevant directions from neurons that are *spuriously active*, i.e. barely above the activation threshold but not corresponding to any salient feature in  $x$ . On the other hand, some important neurons may be inactive, either due to the local noise or because  $x$  is a negative example and does not contain many features relevant to the chosen class  $c$  for which the gradient is computed.

**4.2 Introducing excitation pullbacks**

The considerations from previous section suggest that we should look beyond the hard activation gates  $G(x)$  to properly pull the action of  $y^\top$  back to  $\mathbb{R}^{d_0}$  - in a way that is robust to hyper-local noise. A natural idea is to perform soft gating, i.e. compose the pre-activations  $z_\ell$  with some sigmoid-like step function  $\sigma_\ell : \mathbb{R}^{d_\ell} \rightarrow [0, 1]^{d_\ell}$ :

$$\Gamma : \mathbb{R}^{d_0} \rightarrow \prod_{\ell=1}^L [0, 1]^{d_\ell}, \quad \Gamma := (\gamma_1, \dots, \gamma_L), \quad \gamma_\ell := \sigma_\ell \circ z_\ell : \mathbb{R}^{d_0} \rightarrow [0, 1]^{d_\ell} \quad (21)$$

In general,  $\sigma_\ell$  is neuron-specific, since the pre-activation distribution may be different for each neuron. In practice, thanks to the BatchNorm layers, a shared  $\sigma$  across all neurons yields good empirical results (even though BatchNorm still differentiates between the neuron distributions via it’s affine parameters). In the paper we set the global element-wise  $\sigma_\ell = \sigma = \text{sigmoid}(\frac{z}{0.3}) : \mathbb{R} \rightarrow [0, 1]$ , but other options (e.g. rescaled softsign or Normal CFD) lead to very similar results - as long as the general sigmoid shape of the global  $\sigma$  is preserved, see Section 6.2.

Because  $\sigma_\ell$  can be understood as measuring the *excitation* of a neuron we may accordingly call  $\Gamma$  the *excitation function*, it’s corresponding pullback  $v_\Gamma$  the *excitation pullback*, and it’s induced tensor field  $\tilde{\Gamma}$  the *excitation tensor field*. Note that in order to compute  $\Gamma$  we still need to use the original gates  $G$  in the forward pass to compute the right pre-activations.

**Note 4.2**

The tensor field  $\tilde{\Gamma} : \mathbb{R}^{d_0} \rightarrow \mathbb{R}^{P_1}$  (see Equation 12) suppresses *barely active* paths, i.e. those passing through weakly activated neurons; and partially recovers paths that are *nearly active* (i.e. those interrupted by a single weak neuron, but otherwise strong). This makes  $v_\Gamma$  less sensitive to hyper-local noise across linear regions when compared with  $v_G$  and probably more aligned with the coarser structure of the decision boundary. In a sense,  $v_\Gamma$  is dominated by atoms corresponding to *highly excited* paths, as it quickly suppresses the less-excited paths (see Equation 10).

**5 On the path stability and its potential significance**

**5.1 The path stability hypothesis**

Because of the relative stability of  $\phi_{\tilde{G}^{(t)}}$  (Note 3.3), it’s tempting to assume that the gating function  $G^{(t)}$  gets fixed early on during training. We consider this assumption too optimistic as the gates probably do change simply because of the gradient noise we’ve hinted at before. Notice, however, that  $\tilde{G} : \mathbb{R}^{d_0} \rightarrow \mathbb{R}^{P_1}$  maps inputs to binary rank-1 tensors, meaning that it has limited path-filtering capability (Note 3.1). But perhaps there are more refined atom filters (corresponding to higher-rank binary tensors) that do get fixed early on during training? We motivate this assumption below.

Earlier work has demonstrated that only a small subnetwork within a larger model is responsible for most of its performance. In particular, weight pruning techniques demonstrate that many weights in trained networks can be removed without significantly degrading accuracy, implying the presence of sparse, efficient subnetworks within dense architectures [Han et al., 2015]. Moreover, the Lottery Ticket Hypothesis [Frankle and Carbin, 2019] posits that such performant subnetworks often emerge early during training and can be “rewound” to their initial weights to train successfully in isolation. Furthermore, in [Lakshminarayanan and Singh, 2021] the authors define Neural Path Features (NPF), which are essentially our gating functions (Equation 3), and argue that “almost all the information learnt by a DNN with ReLU activations is stored in the gates”. Specifically, they introduce Deep Gated Networks (DGN) and provide empirical evidence that gate adaptation is the

key to generalization, most notably, that “the winning lottery is in the gating pattern” [Lakshminarayanan and Singh, 2020]. Together, these observations motivate the idea that the gating patterns in ReLU networks may approximately stabilize early in training, and thus may carry semantically meaningful structure long before convergence.

Recall that  $f^{(t)}(x) = \langle \omega^{(t)}, \phi_{\tilde{G}^{(t)}}(x) \rangle$  and  $f_{\pi}^{(t)}(x) = \langle \omega^{(t)}, \phi_{\pi}(x) \rangle$ . Let  $X = (x_i)_i \subset \mathbb{R}^{d_0}$  be the training dataset and  $f(X) = (f(x_i))_i$  be the vector of all the values of  $f$ . We say that two vectors  $a, b \in \mathbb{R}^n$  are *strongly positively correlated* if the Pearson correlation coefficient  $\rho(a, b)$  is high (e.g., greater than 0.9, although the exact threshold value is not important). We denote this relation as  $a \approx_+ b$ . We now state our core hypothesis:

**Hypothesis 1** (Early emergence of stable paths). *There exists a piecewise constant binary tensor field  $\pi : \mathbb{R}^{d_0} \rightarrow \{0, 1\}^{P_1}$  and an early training time  $t_{\pi} \ll T$  such that for every  $t > t_{\pi}$  we have  $f^{(t)}(X) \approx_+ f_{\pi}^{(t)}(X)$ .*

*Additionally, we postulate that the network encodes the tensor field  $\pi$  in its pre-activation function  $Z$ . That is, there exists a choice of  $(\sigma_{\ell})_{\ell}$  (as in Equation 21) such that for every  $x \in X$  we have  $\tilde{\Gamma}(x) \approx_+ \pi(x)$ .*

*We refer to the above assumption as the path stability condition and to any such  $\pi$  as path tensor feature.*

**Intuition:** The hypothesis states that, even though the gating tensors  $\tilde{G}^{(t)}(x)$  change during training, there exists a time-independent gating tensor  $\pi(x)$  that, starting from time  $t_{\pi}$ , largely determines network’s decision  $f^{(t)}(x)$  at  $x$ . In this view, the variability of tensors  $\tilde{G}^{(t)}(x)$  can be attributed to their limited expressive power as rank-1 tensors; the network, trying to approximate  $\pi(x)$ , learns it implicitly in its pre-activation pattern  $Z(x)$  in the form of the set of highly-excited paths. The latter can be feasibly directionally approximated by the rank-1 non-binary tensor  $\tilde{\Gamma}(x)$ .

## 5.2 The implicit kernel machine and the faithfulness of excitation pullbacks

Recall that  $\omega^{(t)} = \Omega((y^{(t)}, \theta^{(t)})) \in \mathbb{R}^{P_0}$  (Equation 16) encodes the network’s parameters at time  $t$  and that:

$$\begin{aligned} f^{(t)}(x) &= \langle \omega^{(t)}, \phi_{\tilde{G}^{(t)}}(x) \rangle \\ f_{\pi}^{(t)}(x) &= \langle \omega^{(t)}, \phi_{\pi}(x) \rangle \end{aligned}$$

If the Hypothesis 1 holds, then, starting from time  $t_{\pi}$  the training dynamics of  $\omega^{(t)}$  closely resembles the training dynamics of the kernel machine given by  $f_{\pi}^{(t)}$ . In fact,  $(\phi_{\tilde{G}^{(t)}} - \phi_{\pi})$  can be interpreted as a *feature noise* added to the fixed feature map  $\phi_{\pi} : \mathbb{R}^{d_0} \rightarrow \mathbb{R}^{P_0}$  at time  $t$  of training.

### Note 5.1

Hypothesis 1 implies that gradient descent actually learns the implicit kernel machine  $f_{\pi}$  and the model  $M$  is just a noisy wrapper that allows us to feasibly approximate the extremely-high-dimensional feature function  $\phi_{\pi}$ .

Since  $\pi$  is assumed to be piecewise constant, then also its pullback  $v_{\pi}$  is piecewise constant and, by Equation 15, we have

$$\nabla f_{\pi}(x) = v_{\pi}^{\top}(x)|_{\mathbb{R}^{d_0}^*} \quad (22)$$

This means that the pullback  $v_{\pi}^{\top}$  can actually be interpreted as the **gradient** of the kernel machine  $f_{\pi}$ . We can feasibly approximate the direction of that gradient by  $v_{\Gamma}$ , which is a better approximation than that of  $v_G$  and therefore  $v_{\Gamma}^{\top}$  is **actually more faithful** to the network’s decision than the standard gradient (if the Hypothesis 1 holds).

Also notice that in order to compute the path space dot product  $\langle \phi_{\Lambda}(x), \phi_{\Lambda}(x') \rangle$  it suffices to compute the following product kernel:

$$K_{\Lambda}(x, x') := \langle x, x' \rangle \prod_{\ell=1}^L \langle \lambda_{\ell}(x), \lambda_{\ell}(x') \rangle = \langle \phi_{\Lambda}(x), \phi_{\Lambda}(x') \rangle, \quad \text{for } x, x' \in \mathbb{R}^{d_0} \quad (23)$$

In particular, we may feasibly study the properties of  $\langle \phi_{\pi}(x), \phi_{\pi}(x') \rangle$  with the help of  $K_{\Gamma}$  kernel. Notice that  $K_{\Gamma}$  encodes the idea behind Deep Features and thus offers a possible explanation for why the latter is an effective perceptual metric [Zhang et al., 2018], as it basically expresses the path-space dot product under the feature map  $\phi_{\pi}$  (up to the scaling), tapping into the internal representation of  $f_{\pi}$ .

## 5.3 The effectiveness of Batch Normalization

Batch Normalization [Ioffe and Szegedy, 2015] has become one of the most influential architectural innovations in modern deep learning, largely due to its ability to dramatically accelerate training and improve generalization. While the standard explanation attributes these benefits to reduced internal covariate shift and smoother optimization landscapes [Santurkar et al., 2019], our framework offers an alternative and complementary perspective.

Note that BN basically removes the bias from inputs and largely prevents the emergence of data-dominant output neurons, enforcing their uniform activation across the batch. This facilitates both the neuron specialization and more uniform usage of the layer width. Highly activated neurons are therefore considerably better aligned (directionally) with the particular input than the less activated ones and have larger impact on the weight update during training, which reinforces their role. All these phenomena favor quicker stabilization of path activations, i.e. faster emergence of the path tensor feature and the corresponding linear structure of network representations, improving the training speed and representational quality.

Interestingly, this resonates with the recent line of work on B-cos networks [Böhle et al., 2022], which explicitly promote weight-input alignment as a mechanism for interpretability. The alignment of excitation pullbacks suggests that the role of B-cos transform is already performed by the BN layer in standard architectures, but this is obfuscated by the pullbacks of weakly excited neurons contaminating the gradient, see Section 4.1.

#### 5.4 ReLU network as content-addressable storage

Under the path stability hypothesis, ReLU networks can be interpreted as an associative memory system with excitation pullbacks as its content. Recall the Note 3.1 where we interpret the pullback vector field  $v_G$  as binary filtering of atoms. This can be understood as computing the target location  $\tilde{G}(x) \in \mathbb{R}^{\mathcal{P}_1}$  in the network’s memory space  $\mathbb{R}^{\mathcal{P}_1}$ . During training, for a positive example  $x$ , the network updates its weights to pull  $v_G^{(t)}(x)$  closer to  $x$  (due to Equation 7), i.e. it combines  $x$  with the value  $v_{G^{(t)}}(x)$  stored at the location  $\tilde{G}^{(t)}(x)$ . Under the path stability condition this location remains largely the same, oscillating around  $\pi(x)$  and therefore  $v_\pi(x)$  (and  $v_\Gamma(x)$ ) contains the most coherent information. This is validated by the perceptual alignment of excitation pullbacks.

During inference, the network first computes the location  $\tilde{G}(x)$  and then takes the dot product of  $x$  with the stored memories  $v_{(c,G)}(x)$  for every class  $c$ , returning the class of the best-matching memory. According to the path stability hypothesis, we can extract the actual memories by computing  $v_{(c,\Gamma)}(x)$  instead (the excitation pullback for class  $c$ ). It may however change the network’s prediction if the pullbacks weren’t used during the training.

## 6 Empirical validation

This section describes how we visualize the excitation pullbacks. To this end, we focus on popular and representative classes of ReLU-based architectures pretrained on ImageNet and available via the `torchvision` library, such that it is straightforward to replace most or all occurrences of ReLU and MaxPool2d (see Section 6.3) layers with our alternative variants, using a single recursive function over the child modules. Based on these criteria, we selected **ResNet50**, **VGG11\_BN**, and **DenseNet121**.

Notably, determining the optimal choice of  $\sigma_\ell$  for every neuron or layer in a given network is outside the scope of this work. Instead, we seek a single global set of hyperparameters that performs reasonably well across all layers of a given model - and ideally, across all selected architectures. Our goal is to evaluate whether the resulting excitation pullbacks indeed exhibit a substantially improved perceptual alignment compared to standard gradients.

### 6.1 Experimental setup

To generate visualizations, we use the `val` split of the publicly available *Imagenette* dataset [Howard, 2019], a subset of ImageNet containing 10 easily recognizable classes. To simplify presentation, we select every other class from the dataset, i.e.: *tench*, *cassette player*, *church*, *garbage truck*, and *golf ball*.

For each visualization, we construct a batch containing one random image from each of the five selected classes. We then compute *excitation pullbacks* for the classification neuron  $y_c$  corresponding to each class, producing a  $5 \times 5$  grid: each row corresponds to an input image, and each column to the target class for which the pullback is computed. We also compute the pullback for a randomly selected ImageNet class (“ostrich”), shown in the last column.

We repeat the same setup, but instead of computing a single excitation pullback, we perform a rudimentary projected gradient ascent toward the logit (pre-activation) of each class, along the excitation pullback. We perform the gradient ascent with images rescaled to the  $[-1, 1]$  range (and then appropriately normalized before feeding to the model). Specifically, at each iteration we take a gradient step of  $L_2$ -norm 20, whose direction is given by the excitation pullback. At each step we project the perturbed image on the ball of radius  $\epsilon = 100$  centered at the original image. We iterate this process 10 times and plot both the final perturbed images and their differences from the originals. For contrast, we repeat the same procedure using vanilla input gradients in place of excitation pullbacks. Note that due to the choice of  $\epsilon$ , the perturbations are roughly fixed after 5 iterations (see Figure 1), the other 5 serving to further refine the perturbations and make them visually clearer.

### 6.2 Technical details

We can easily compute the excitation pullback  $v_\Gamma$  by first computing the right pre-activations  $z_\ell$  via  $M_G$  (doing the ordinary forward pass) and then multiplying ReLU gradients by  $\sigma_\ell(z_\ell)$  in the backward pass, i.e. computing *surrogate gradients* for

ReLU layers. This can be achieved in PyTorch [Paszke et al., 2019] by defining the appropriate `torch.autograd.Function`, see Listing 1. Alternatively, the more flexible Forward Gradient Injection can be used [Otte, 2024].

In the experiments we use a fixed global  $\sigma$  for all the layers in all the networks, but ideally  $\sigma_\ell$  could be adjusted for every hidden neuron separately, based on the neuron pre-activation distribution. We’ve observed that different choices of the global  $\sigma$  produced similarly-looking pullback visualizations as long as the overall sigmoidal shape of the global  $\sigma$  function remained the same. We’ve chosen  $\sigma(z) = \text{sigmoid}(\frac{z}{\text{temp}})$  for `temp = 0.3` but any selection of the parameter `temp` from the approximate range `temp ∈ [0.15, 0.5]` seemed to work quite well *across all the tested architectures*, which implies the considerable robustness of the method to the hyperparameter choice. Notice that  $\Gamma$  approaches hard gating  $G$  as `temp` goes to zero and no gating at all as `temp` goes to infinity.

We use `resnet50`, `vgg11_bn` and `densenet121` models with the flag `pretrained=True` from the `torchvision.models` library.<sup>5</sup> Gradients are visualised by `torchvision.utils.make_grid(scale_each=True)`. We seed the dataloader with `torch.Generator().manual_seed(314)`.

### 6.3 Excitation pullbacks through the MaxPool2d layer

Most convolutional architectures use spatial non-linearities in the form of MaxPool2d layers which can be viewed as a generalization of ReLU, i.e.  $\text{ReLU}(z) = \max(0, z)$  and both operations propagate gradients only through the local maxima. This motivates the application of surrogate gradients to these layers as well. Analogously to the excitation pullback modification for ReLU, we leave the forward pass of max pooling unchanged, but replace its gradient with that of a *softmax* pooling operation, using the strike-through trick. This indeed smoothens the pullbacks even further. Implementation details can be found in the Listing 2; we set the temperature parameter to 0.3, the same as in surrogate gradient for ReLU.

### 6.4 Plotting excitation pullbacks

We present the plots generated according to the procedure described in Section 6.1, i.e. Figures 2, 3 and 4. As shown in the experiments, a single global choice of the function  $\sigma$  performs reasonably well across all considered architectures, indicating a substantial robustness of excitation pullbacks to hyperparameter selection. As noted in Section 6.2, the visualizations remain qualitatively similar across a wide range of  $\sigma$  choices. Moreover, excitation pullbacks tend to highlight similar features across architectures, which suggests that the models learn comparable feature representations. Finally, the structure of the excitation pullbacks intuitively reflects the internal organization of each network, reinforcing our hypothesis that they indeed faithfully capture the underlying decision process of the model.

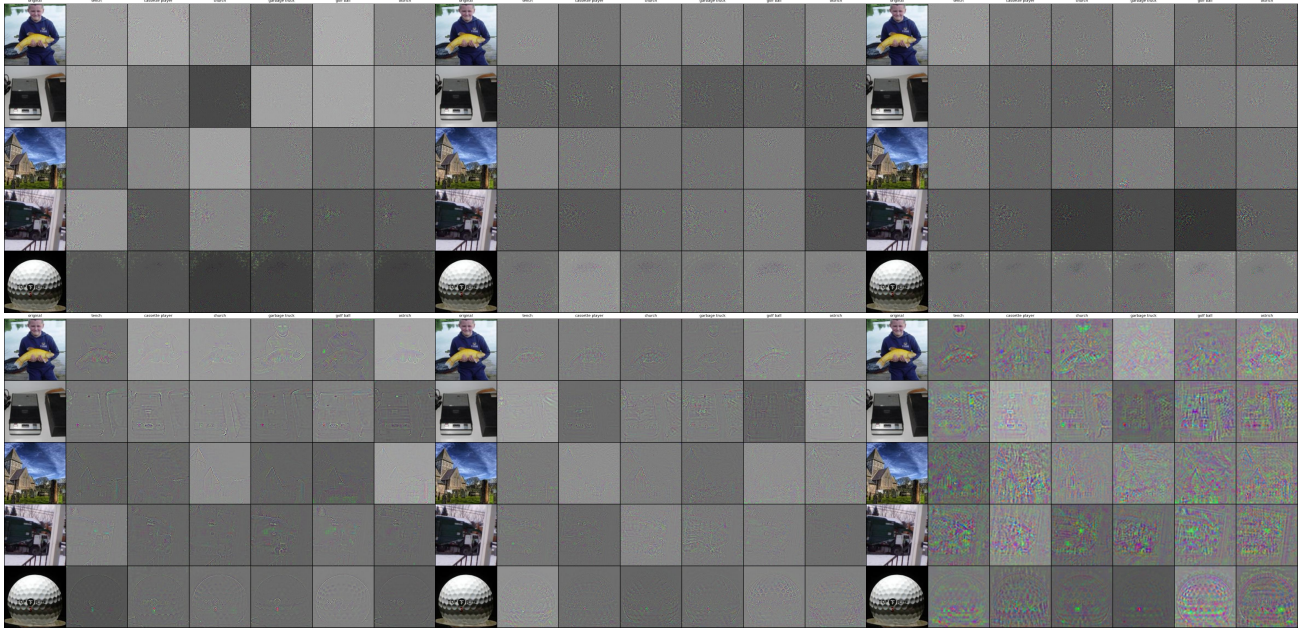


Figure 2: Top row: vanilla gradients; bottom row: excitation pullbacks. From left to right: ResNet50, VGG11\_BN, DenseNet121. Best viewed digitally.

<sup>5</sup>see Section 7.3 for more context.

## 7 Discussion

### 7.1 Related work

Similar approach to ReLU networks from the path perspective has appeared in [Yadav et al., 2024] where authors study the so-called Deep Linearly Gated Networks (DLGN) in which the gating function  $G$  is computed by a parallel *linear* model  $M$  with independent set of parameters  $\theta$ . They show that such models are considerably more interpretable than standard DNN’s and retain much of their performance. We highlight the authors’ other relevant contributions in Section 5.1, motivating our Hypothesis 1. Overall, they arrive at similar formal constructions throughout their works but their main focus is on alternative architectures like DGNs; in contrast, we present a refined formal framework to study properties of standard architectures.

In [Linse et al., 2024] it is shown that setting the negative slope of LeakyReLU considerably higher in the backward pass than the forward pass leads to much better aligned global feature visualisations via activation maximization, which can be directly explained by our results as LeakyReLU is equivalent to setting constant excitation function for each of the real half-lines (e.g. 1 for positive values and 0.3 for non-positive). In [Horuz et al., 2025] they generalize this idea to ReLU’s with different surrogate gradients, which is even closer to our approach, indicating that particular selection of surrogate ReLU gradient (e.g. B-SiLU) consistently improves generalization performance. Combined with our findings this leads to the open question, whether computing excitation pullbacks (instead of vanilla gradients) during training can improve generalization, and to what extent. Intuitively, one should not differentiate through the excitation gates explicitly as they may saturate and overfit; nevertheless, they can still be computed in the backward pass as alternative gradients.

Another closely related work concerns local *feature accentuations*, [Hamblin et al., 2024] where authors obtain high-quality local feature visualizations that are specific to the seeded image and the target feature. Furthermore, they argue that these accentuations are processed by the model along its natural circuit. Even though the produced images are of remarkably high quality, the proposed method uses strong image regularizations during the gradient ascent (in particular, images need to be transformed to the frequency domain) and requires as much as 100 gradient steps. Furthermore, the faithfulness of the produced explanations is established intuitively, without referencing the training dynamics.

It has been observed that networks trained to be robust to adversarial perturbations yield gradients that are often aligned with human perception, a phenomenon first observed in [Tsipras et al., 2019] and then referred to as *perceptually-aligned gradients* (PAG) in [Kaur et al., 2019]. In [Srinivas et al., 2024] the authors attribute the PAG property to *off-manifold robustness*, which leads input gradients to lie approximately on the data manifold. This resonates with our observation that excitation pullback  $v_{\Gamma}$  provides a smoother approximation of the model’s decision boundary than the standard, hard-gated gradients and therefore, by extension, may better align with the actual data manifold.

### 7.2 On the possible biological plausibility of the implicit linear model

Intuitively, the relative stability of the gating mechanism throughout training is reminiscent of the approximately fixed synaptic connections observed in biological neural systems. In this analogy, the discrete gating pattern can be thought of as defining a persistent connectivity structure - akin to neural connections - while the excitation function describes the level of activity (excitation) of each neuron, resembling the frequency-based coding of information.

One may even venture a more speculative interpretation: the excitation pullbacks could be loosely associated with internal subjective representations, i.e. *qualia* - subjective, localized manifestations of experience that emerge from the brain activity taken as a whole - in a way similar to how excitation pullbacks emerge from the gating patterns in ReLU networks. It makes even more sense in the light of Section 5.4, where we interpret excitation pullbacks as the content of the network’s associative memory. This may open exciting direction in neuroscience and the philosophy of mind.

### 7.3 Limitations

Our experiments were run on pretrained `torchvision` models downloaded with the flag `pretrained=True`. This flag is now deprecated in the recent versions of the library, in particular it returns the older `ResNet50_Weights.IMAGENET1K_V1`. We’ve observed that it’s harder (but still possible) to achieve similar quality of excitation pullbacks for the more recent `ResNet50_Weights.IMAGENET1K_V2` weights, at least when using a single global  $\sigma$  for all the neurons, which, as we’ve indicated earlier, might be an oversimplified approach. We speculate that this is because of different distribution of pre-activations in newer versions of the pretrained models, which have been heavily regularized.

The formal theory developed in this paper concerns specifically the ReLU networks. Intuitively, similar arguments should hold for other activation functions, in particular the ones similar to ReLU, e.g. SiLU and GELU. Initial experiments for those architectures show promise but require certain refinement of the computation of  $\Gamma$  to account for the more complex gradients. We haven’t yet explored the potential applicability of our method to attention-based models.

Additionally, we expect the convolutions to play rather significant role in the emergence of aligned excitation pullbacks, as spatial weight sharing seems to be crucial for the early path stabilization. This underlines the importance of an appropriate inductive bias for our results to carry over to other domains.

## 8 Acknowledgments

This research was conducted at the 314 Foundation<sup>6</sup> with support from a private grant awarded specifically for this study.

## References

- Moritz Böhle, Mario Fritz, and Bernt Schiele. B-cos networks: Alignment is all we need for interpretability, 2022. URL <https://arxiv.org/abs/2205.10268>.
- Nick Cammarata, Shan Carter, Gabriel Goh, Chris Olah, Michael Petrov, Ludwig Schubert, Chelsea Voss, Ben Egan, and Swee Kiat Lim. Thread: Circuits. *Distill*, 2020. doi: 10.23915/distill.00024. <https://distill.pub/2020/circuits>.
- Chaofan Chen, Oscar Li, Chaofan Tao, Alina Jade Barnett, Jonathan Su, and Cynthia Rudin. This looks like that: Deep learning for interpretable image recognition, 2019. URL <https://arxiv.org/abs/1806.10574>.
- Jonathan Frankle and Michael Carbin. The lottery ticket hypothesis: Finding sparse, trainable neural networks, 2019. URL <https://arxiv.org/abs/1803.03635>.
- Chris Hamblin, Thomas Fel, Srijani Saha, Talia Konkle, and George Alvarez. Feature accentuation: Revealing 'what' features respond to in natural images, 2024. URL <https://arxiv.org/abs/2402.10039>.
- Song Han, Jeff Pool, John Tran, and William J. Dally. Learning both weights and connections for efficient neural networks, 2015. URL <https://arxiv.org/abs/1506.02626>.
- Kaiming He, Xiangyu Zhang, Shaoqing Ren, and Jian Sun. Deep residual learning for image recognition, 2015. URL <https://arxiv.org/abs/1512.03385>.
- Coşku Can Horuz, Geoffrey Kasenbacher, Saya Higuchi, Sebastian Kairat, Jendrik Stoltz, Moritz Pesl, Bernhard A. Moser, Christoph Linse, Thomas Martinetz, and Sebastian Otte. The resurrection of the relu, 2025. URL <https://arxiv.org/abs/2505.22074>.
- Jeremy Howard. Imagenette and imagewoof: Subsets of imagenet for quick experiments. <https://github.com/fastai/imagenette>, 2019. Accessed: 2025-07-21.
- Gao Huang, Zhuang Liu, Laurens van der Maaten, and Kilian Q. Weinberger. Densely connected convolutional networks, 2018. URL <https://arxiv.org/abs/1608.06993>.
- Sergey Ioffe and Christian Szegedy. Batch normalization: Accelerating deep network training by reducing internal covariate shift, 2015. URL <https://arxiv.org/abs/1502.03167>.
- Simran Kaur, Jeremy Cohen, and Zachary C. Lipton. Are perceptually-aligned gradients a general property of robust classifiers?, 2019. URL <https://arxiv.org/abs/1910.08640>.
- Chandrashekar Lakshminarayanan and Amit Vikram Singh. Deep gated networks: A framework to understand training and generalisation in deep learning, 2020. URL <https://arxiv.org/abs/2002.03996>.
- Chandrashekar Lakshminarayanan and Amit Vikram Singh. Neural path features and neural path kernel : Understanding the role of gates in deep learning, 2021. URL <https://arxiv.org/abs/2006.10529>.
- Christoph Linse, Erhardt Barth, and Thomas Martinetz. Leaky relus that differ in forward and backward pass facilitate activation maximization in deep neural networks. In *2024 International Joint Conference on Neural Networks (IJCNN)*, page 1–8. IEEE, June 2024. doi: 10.1109/ijenn60899.2024.10650881. URL <http://dx.doi.org/10.1109/IJCNN60899.2024.10650881>.
- Sebastian Otte. Flexible and efficient surrogate gradient modeling with forward gradient injection, 2024. URL <https://arxiv.org/abs/2406.00177>.
- Adam Paszke, Sam Gross, Francisco Massa, Adam Lerer, James Bradbury, Gregory Chanan, Trevor Killeen, Zeming Lin, Natalia Gimelshein, Luca Antiga, Alban Desmaison, Andreas Köpf, Edward Yang, Zach DeVito, Martin Raison, Alykhan Tejani, Sasank Chilamkurthy, Benoit Steiner, Lu Fang, Junjie Bai, and Soumith Chintala. Pytorch: An imperative style, high-performance deep learning library, 2019. URL <https://arxiv.org/abs/1912.01703>.
- Shibani Santurkar, Dimitris Tsipras, Andrew Ilyas, and Aleksander Madry. How does batch normalization help optimization?, 2019. URL <https://arxiv.org/abs/1805.11604>.
- Karen Simonyan and Andrew Zisserman. Very deep convolutional networks for large-scale image recognition, 2015. URL <https://arxiv.org/abs/1409.1556>.
- Suraj Srinivas, Sebastian Bordt, and Hima Lakkaraju. Which models have perceptually-aligned gradients? an explanation via off-manifold robustness, 2024. URL <https://arxiv.org/abs/2305.19101>.
- Dimitris Tsipras, Shibani Santurkar, Logan Engstrom, Alexander Turner, and Aleksander Madry. Robustness may be at odds with accuracy, 2019. URL <https://arxiv.org/abs/1805.12152>.
- Mahesh Lorik Yadav, Harish Guruprasad Ramaswamy, and Chandrashekar Lakshminarayanan. Half-space feature learning in neural networks, 2024. URL <https://arxiv.org/abs/2404.04312>.
- Richard Zhang, Phillip Isola, Alexei A. Efros, Eli Shechtman, and Oliver Wang. The unreasonable effectiveness of deep features as a perceptual metric, 2018. URL <https://arxiv.org/abs/1801.03924>.

---

<sup>6</sup><https://314.foundation>

Listing 1: PyTorch implementation of the backward pass through ReLU

```

import torch
import torch.nn as nn
import torch.nn.functional as F

class TwoWayReLUFunction(torch.autograd.Function):
    @staticmethod
    def forward(ctx, z, temperature=0.3):
        ctx.save_for_backward(z)
        ctx.temperature = temperature
        return F.relu(z)

    @staticmethod
    def backward(ctx, grad_output):
        (z,) = ctx.saved_tensors
        temp = ctx.temperature

        gate = F.sigmoid(z / temp)

        return grad_output * gate, None

```

Listing 2: PyTorch implementation of the backward pass through MaxPool2d

```

class SoftMaxPool2d(nn.MaxPool2d):
    def __init__(self, *args, temperature=0.3, **kwargs):
        super(()).__init__(*args, **kwargs)
        self.temperature = temperature

    def forward(self, x):
        B, C, H, W = x.shape
        kH, kW = self.kernel_size, self.kernel_size

        # Unfold input to patches
        x_unf = F.unfold(x, kernel_size=self.kernel_size,
                        stride=self.stride, padding=self.padding)
        x_unf = x_unf.view(B, C, kH * kW, -1)

        # Softmax pooling over spatial positions
        weights = F.softmax(x_unf / self.temperature, dim=2)
        pooled = (x_unf * weights).sum(dim=2)

        # Reshape back to image
        out_H = (H + 2*self.padding - kH) // self.stride + 1
        out_W = (W + 2*self.padding - kW) // self.stride + 1
        return pooled.view(B, C, out_H, out_W)

class SurrogateSoftMaxPool2d(SoftMaxPool2d):
    def forward(self, x):
        soft = super(()).forward(x)
        hard = F.max_pool2d(x, self.kernel_size, self.stride,
                           self.padding, self.dilation,
                           ceil_mode=self.ceil_mode,
                           return_indices=self.return_indices)
        return hard.detach() + (soft - soft.detach())

```

# Pulling back the curtain on ReLU networks



Figure 3: Left: Image perturbations after 10-step projected gradient ascent along excitation pullbacks toward each of the classes (columns). Right: Difference between the perturbed and original images. From top to bottom: ResNet50, VGG11\_BN, DenseNet121. One can clearly distinguish label-specific features highlighted by the model on every image. Compare with the same plots for vanilla gradients, Figure 4. Best viewed digitally.

Pulling back the curtain on ReLU networks



Figure 4: Left: Image perturbations after 10-step projected gradient ascent along vanilla gradients toward each of the classes (columns). Right: Difference between the perturbed and original images. From top to bottom: ResNet50, VGG11\_BN, DenseNet121. The features are barely discernible. Compare with the same plots for excitation pullbacks, Figure 3